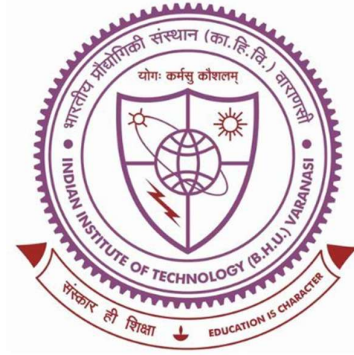


# Effect of Heat Treatments and Electropulsing on the Microstructure and Mechanical Properties of Austenite Based Low-Density Steels



Thesis submitted in partial fulfillment for the  
Award of Degree

**Doctor of Philosophy**

By

**Rajavarapu Pavan Kumar**

DEPARTMENT OF METALLURGICAL ENGINEERING  
INDIAN INSTITUTE OF TECHNOLOGY  
(BANARAS HINDU UNIVERSITY)  
VARANASI-221005  
INDIA

18141007

2025

# CERTIFICATE

It is certified that the work contained in the thesis titled "**Effect of Heat Treatments and Electropulsing on the Microstructure and Mechanical Properties of Austenite Based Low-Density Steels**" by Rajavarapu Pavan Kumar has been carried out under our supervision and that this work has not been submitted elsewhere for a degree.

It is further certified that the student has satisfactorily fulfilled all the requirements of Comprehensive Examination, Candidacy, SOTA, Pre-submission seminar for the award of the Ph.D. degree.



Prof. Rampada Manna

(Supervisor)

Department of Metallurgical Engineering

IIT (BHU), Varanasi-221005

प्राचार्य / Professor

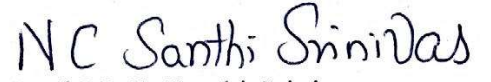
धातुकीय अभियांत्रिकी विभाग

Department of Metallurgical Engg.

भारतीय प्रौद्योगिकी संस्थान (काशी हिन्दू विश्वविद्यालय)

Indian Institute of Technology (Banaras Hindu University)

वाराणसी-221005/Varanasi-221005



Prof. N. C. Santhi Srinivas

(Co-Supervisor)

Department of Metallurgical Engineering

IIT (BHU), Varanasi-221005

प्राचार्य / Professor

धातुकीय अभियांत्रिकी विभाग

Department of Metallurgical Engg.

भारतीय प्रौद्योगिकी संस्थान (काशी हिन्दू विश्वविद्यालय)

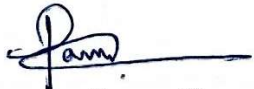
Indian Institute of Technology (Banaras Hindu University)

वाराणसी-221005/Varanasi-221005

## DECLARATION BY THE CANDIDATE


I, "Rajavarapu Pavan Kumar", certify that the work embodied in this thesis is my own bona fide work and carried out by me under the supervision of Prof. Rampada Manna and Prof. N. C. Santhi Srinivas from "2018" to "2025", at the Department of Metallurgical Engineering, Indian Institute of Technology (BHU), Varanasi. The matter embodied in this thesis has not been submitted for the award of any other degree/diploma. I declare that I have faithfully acknowledged and given credits to the research workers wherever their works have been cited in my work in this thesis. I further declare that I have not willfully copied any other's work, paragraphs, text, data, results, etc., reported in journals, books, magazines, reports dissertations, theses, etc., or available at websites and have not included them in this thesis and have not cited as my own work.

Date: 27/02/2025  
Place: Varanasi

  
Rajavarapu Pavan Kumar  
(Candidate)

## CERTIFICATE BY THE SUPERVISOR(S)

It is certified that the above statement made by the student is correct to the best of my/our knowledge.

  
Prof. Rampada Manna  
(Supervisor)  
प्राचार्य / Professor

धातुकीय अभियांत्रिकी विभाग  
Department of Metallurgical Engg.  
भारतीय प्रौद्योगिकी संस्थान (काशी हिन्दू विश्वविद्यालय)  
Indian Institute of Technology (Banaras Hindu University)  
वाराणसी-221005/Varanasi-221005

NC Santhi Srinivas  
Prof. N. C. Santhi Srinivas  
(Co-Supervisor)  
प्राचार्य / Professor

धातुकीय अभियांत्रिकी विभाग  
Department of Metallurgical Engg.  
भारतीय प्रौद्योगिकी संस्थान (काशी हिन्दू विश्वविद्यालय)  
Indian Institute of Technology (Banaras Hindu University)  
वाराणसी-221005/Varanasi-221005

NC Santhi Srinivas  
Head of the Department  
विभागाध्यक्ष / HEAD  
धातुकीय अभियांत्रिकी विभाग  
Department of Metallurgical Engg.  
भारतीय प्रौद्योगिकी संस्थान (काशी हिन्दू विश्वविद्यालय)  
Indian Institute of Technology (Banaras Hindu University)  
वाराणसी-221005/Varanasi-221005

# **COPYRIGHT TRANSFER CERTIFICATE**

Title of the Thesis: **Effect of Heat Treatments and Electropulsing on the Microstructure and Mechanical Properties of Austenite Based Low-Density Steels**

Name of the Student: **Rajavarapu Pavan Kumar**

## **COPYRIGHT TRANSFER**

The undersigned hereby assigns to the Institute of Technology (Banaras Hindu University) Varanasi all rights under copyright that may exist in and for the above thesis submitted for the award of the PhD degree.

Date: 27/02/2025  
Place: Varanasi

  
(Rajavarapu Pavan Kumar)

Note: However, the author may reproduce or authorize others to reproduce material extracted verbatim from the thesis or derivative of the thesis for author's personal use provided that the source and the Institute's copyright notice are indicated.

## ACKNOWLEDGEMENTS

I am deeply grateful and indebted to my supervisors, **Prof. Rampada Manna** and **Prof. N. C. Santhi Srinivas**, for their unwavering support, encouragement, and invaluable guidance throughout the course of my research. Their faith in my abilities, constant motivation, and insightful discussions have been instrumental in shaping the direction of this work. Their dedication and mentorship were pivotal in helping me navigate the challenges and in reinforcing the importance of persistence in research.

I would like to sincerely thank the RPEC committee members, Prof. Joysurya Basu and Prof. Mohd Zaheer Khan Yusufzai, for their thoughtful suggestions and continuous encouragement. I am also highly grateful to Prof. N. C. Santhi Srinivas, Head of the Department, and to the former Heads, Prof. Sunil Mohan, Prof. N. K. Mukhopadhyay, and Prof. R. K. Mandal, for their support and guidance. I extend my heartfelt thanks to Prof. B. N. Sharma, Prof. O. P. Sinha, Prof. K. Chattopadhyay, Prof. N. K. Prasad, Dr. Sudipta Patra, Dr. Subhasis Sinha, Dr. S. D. Yadav, Dr. Harsha Nandam, Dr. Sake Narayana Swami and all faculty members for their valuable inputs and enriching discussions during coursework and beyond. I would also like to acknowledge Prof. R. K. Pandey for his insightful suggestions on electropulsing.

I am thankful to the Advanced Research Centre for Iron and Steel, funded by the Ministry of Steel, Government of India, for providing access to the Induction Melting Furnace and X-ray diffractometer facility. I also gratefully acknowledge the Central Instrument Facility Centre (CIFC), IIT (BHU), for extending various analytical facilities crucial to my research. My sincere appreciation goes to the lab staff—Lalit Kumar Singh, Anjani Singh, Ramashray Yadav, Kamalesh Ji, Minz Ji, Patel Ji and Rana Ji—and to the office staff of the department for their consistent support and cooperation.

The memorable moments, peer learning, and camaraderie with my seniors—Dr. Raj Bahadur Singh, Dr. Debabrata Bhuyan, Dr. Sandeep, Dr. Jaydeep, and Dr. Roopchand Tandon—along with the friendship and support from my batchmates—Manish Tiwari and Hemant Kumar—and juniors—Sourajit Pramanik and Abhay Singh—were a continuous source of strength and inspiration. I am especially thankful to my other departmental seniors—Charan anna, Ramakrishna anna, Krishna anna, and Venkateswarlu anna—who have supported me with their guidance, encouragement, and practical advice right from the very first year of my Ph.D.

A heartfelt thanks to Rajavarapu Srinivasa Rao, whose emotional support during trying times gave me strength and hope.

Above all, I wish to express my deepest gratitude to my **family**, whose unwavering love and sacrifices made this journey possible. My **parents, Rajavarapu Purna Chandra Rao and Narasamma**, have been the foundation of my values and perseverance. Their lifelong encouragement, silent prayers, and unconditional love have sustained me through every high and low. My **brother, Anil Kumar**, has always stood by me as a pillar of strength. My **wife, Bhulakshmi**, has been my constant companion, offering endless patience, encouragement, and emotional resilience, without which this accomplishment would not have been possible. Finally, my **children, Sagarika and Abhinav Antony**, are my greatest source of joy and motivation—their innocent smiles and unconditional love gave me the courage to keep moving forward, even during the toughest days. I also thank the Lord for His grace, guidance, and unfailing love throughout this journey. In times of doubt and difficulty, His presence was my strength and refuge. It is through His divine will that I have been able to reach this milestone.

**With all my heart, I dedicate this thesis to my family.** Their support, belief, and sacrifices are the true foundation of this achievement.

## LIST OF TABLES

Table 1.1: Mechanical properties of austenitic steels .....	55
Table 1.2: Properties of Commonly Used Ceramic Reinforcements and Metallic Matrix Materials .....	61
Table 1.3: Processing, microstructure, and tensile properties of Ni-added low-density steels .....	65
Table 2.1: Designed compositions (all by mass %).....	73
Table 2.2: Analyzed compositions of PD1, PD2 and PD3 .....	79
Table 2.3: Electropulsing parameters .....	82
Table 2.4: Integral breadth of standard Silicon.....	85
Table 3.1: Density, elastic modulus, shear modulus, and Poisson ratio of PD1-S steel...	94
Table 3.2: Strengthening contributions from various mechanisms to yield strength. ....	100
Table 3.3: Strength coefficients, work-hardening exponents and fitting parameters with Ludwigson flow equation for PD1-S. ....	103
Table 3.4: Microstructural data of PD1-SC and PD1-SCR samples .....	110
Table 3.5: Tensile properties of PD1-SC and PD1-SCR samples. ....	115
Table 3.6: Tensile properties of PD1-SCR tested at various strain rates.....	115
Table 3.7: Fractography analysis of PD1-SCR samples at various strain rates.....	116

Table 3.8: Contribution of strengthening mechanisms to yield strength of PD1-SC and PD1-SCR samples.....	117
Table 3.9: Work hardening parameters of PD1-SC and PD1-SCR samples .....	119
Table 4.1: Density, Elastic modulus, Shear modulus, and Poisson ratio of PD2-S.....	125
Table 4.2: Contribution of strengthening mechanisms to yield strength of PD2-S. ....	135
Table 4.3: Strength coefficients, work-hardening exponents and fitting parameters with Ludwigson flow equation for PD2-S. ....	138
Table 5.1: Crystallite size, micro strain, and dislocation densities of austenite and B2 phases in PD3, PD3-A, and PD3-AB <sub>30</sub> samples.....	148
Table 5.2: Vickers hardness of PD3-A samples aged at 550°C.....	149
Table 5.3: Composition of features derived from the EDS spectrum.....	150
Table 5.4: Tensile properties of PD3, PD3-A and PD3-AB <sub>30</sub> low-density steels.....	162
Table 5.5: Work hardening rate at the start and the true strain at the end of stages I, II, and III for PD3, PD3-A, and PD3-AB <sub>30</sub> .....	162
Table 5.6: Strength coefficients, work-hardening exponents, and fitting parameters with Ludwigson flow equation for PD3, PD3-A, and PD3-AB <sub>30</sub> samples.....	163
Table 5.7: Size of dimples and facets in fractographs .....	165
Table 5.8: Contribution of different strengthening mechanisms to yield strength .....	177
Table 5.9: Comparison of Tensile properties of a few commercial steels to newly developed low-density steels.....	184

Table 6.1: LAGB and HAGB fractions, average MA and KAM values of B2 and austenite .....	196
Table 6.2: Work hardening parameters.....	221
Table 6.3: Sizes of different B2 morphologies before and after electropulsing .....	226
Table 6.4: Volume fraction and dislocation density values of PD3-AB <sub>30</sub> and PD3-AB <sub>30</sub> E samples.....	228
Table 6.5:LAGB and HAGB fractions, average MA and KAM values of B2 and austenite .....	234
Table 6.6: Tensile properties of PD3-AB <sub>30</sub> , PD3-AB <sub>30</sub> E samples.....	235
Table 6.7: Tensile properties of PD3-A, PD3-AE, PD3-AB <sub>30</sub> and PD3-AB <sub>30</sub> E samples	240

## LIST OF FIGURES

Figure 1.1: Banana Diagram depicting the strength and elongation characteristics of various steel Grades .....	42
Figure 1.2: Illustrative Representation of the Body in White Structure of the 2015 Ford Edge Vehicle and the Corresponding Mass Distribution of Materials. ....	43
Figure 1.3: Relationship between density and aluminum concentration (mass %) in iron-aluminum alloys .....	44
Figure 1.4: Process variants for producing austenite-based Fe-Mn-Al-C steel strips. The numbers identify process routes as described in the text .....	49
Figure 1.5: (a) TEM BF image of intra-granular kappa carbide precipitate (b) Corresponding diffraction pattern and (c) Simulated diffraction pattern of kappa carbide with respect to austenite matrix (d) Transmission electron Bright Field image of inter-granular kappa carbide precipitate along with ferrite (e) corresponding diffraction pattern (f) Simulated diffraction pattern of kappa carbide with respect to ferrite.. ....	51
Figure 1.6: A comparative illustration depicting the impact of different precipitates on strength contribution in MPa relative to the volume fraction of kappa carbide precipitation. ....	54
Figure 1.7: (a) Hall–Petch relationship in ultrafine grained bcc steels (b) Grain size dependence of ductility for bcc steels .....	58
Figure 1.8: Effect of aluminum content on Young's Modulus of low-density steels. ....	59

Figure 1.9: (a) SEM micrograph of different types of B2 precipitates in austenite matrix  
(b) TEM micrograph and corresponding diffraction pattern of B2 along zone axis of [110]  
.....63

Figure 2.1: Vacuum induction melting furnace facility at ARCIS centre. ....75

Figure 2.2: (a) copper mould (b) dimensions of half side of copper mould (c) cast plate.75

Figure 2.3: Schematic representation of (a)Thermomechanical processing followed by  
annealing treatment for P1, P2 (b) cold rolling followed by repeated annealing treatment  
of PD1-S.....77

Figure 2.4: Schematic representation of thermomechanical process followed by annealing  
and aging treatments. ....78

Figure 2.5: (a) Electropulsing sample with (1) clamping region and (2) area for  
microstructural and tensile characterization (b) Schematic of the electropulsing (EP) setup,  
EP output waveform (c) for PD3-A, (d) for PD3-AB<sub>30</sub> (where 1 division in waveform on  
y-axis is 1V, which is equivalent to 100 kA of output current. 1 division on x-axis is 50 μs)  
.....82

Figure 2.6: Electropulsing facility in Metallurgical Engineering department. ....83

Figure 2.7: Tensile specimen with dimensions according to ASTM E8-04.....88

Figure 3.1: Calculated phase diagram of selected alloy using ThermoCalc software,  
illustrating phase stability regions as a function of temperature and aluminum  
concentration.....93

Figure 3.2: (a) Optical micrograph (b) XRD pattern of PD1-S. ....95

Figure 3.3: (a) IQ map (b) Grain size vs area fraction chart of PD1-S.....	96
Figure 3.4: (a) Engineering stress-strain curve of PD1-S and its (b) SEM fractograph ....	98
Figure 3.5: (a) Logarithmic true stress vs. logarithmic true plastic strain plots of PD1-S fitted with various models, (b) Work hardening rate vs true plastic stress diagram.....	102
Figure 3.6: Linear fitting curves of the third stage in PD1-S using Kock, Mecking, (KM) based dislocation models. ....	105
Figure 3.7: IQ maps of (a) PD1-SC and (c) PD1-SCR samples, grain size vs. area fraction charts for (b) PD1-SC, and (f) PD1-SCR samples.....	108
Figure 3.8: KAM maps of (a) PD1-SC and (b) PD1-SCR samples.....	109
Figure 3.9: IQ maps with superimposed grain boundaries of (a) PD1-SC and, (b) PD1-SCR samples.....	111
Figure 3.10: $\phi_2 = 0^\circ, 45^\circ$ and $65^\circ$ sections of orientation distribution functions (ODFs) of austenite phase in (a) PD1-SC sample and (d) PD1-SCR sample (RG= Rotated Goss, RW= Rotated W). ....	112
Figure 3.11: Engineering stress-strain curves of (a) PD1-SC, and PD1-SCR samples at $10^{-3}/s$ strain rate (b) Engineering tensile stress-strain curves for PD1-SCR samples tested at strain rates of $10^{-3}/s, 10^{-2}/s, 10^{-1}/s, 10^0/s$ . ....	114
Figure 3.12: Fracture morphologies of PD1-SCR samples tested at strain rates of (a) $10^{-3}/s$ , (b) $10^{-2}/s$ , (c) $10^{-1}/s$ , (d) $10^0/s$ . ....	116
Figure 3.13: Work hardening rate vs true plastic strain diagrams of PD1-SC and PD1-SCR samples.....	119

Figure 4.1: Phase fraction diagram of PD2 with the amount of all phases with respect to temperature. .... 124

Figure 4.2: (a) Optical micrographs of PD2-S, (b) XRD pattern of PD2-S. SEM secondary electron micrograph of PD2-S (c) at 5000X showing TiC particles on which EDS spectrum is taken (d) EDS spectrum of TiC particle sh shown in Figure 4.2(c), (e) at 1000X showing TiC particle distribution (f) SEM secondary electron micrograph of PD2-S at 2500X and (g) TiC particle size distribution chart of Figure 4.2(f). .... 128

Figure 4.3: (a) IQ map, (b) grain size vs area fraction chart of PD2-S..... 130

Figure 4.4: (a) Engineering stress- plastic strain curve of PD2-S and its (b) SEM secondary electron image of fracture surface..... 131

Figure 4.5: (a) Logarithmic true stress vs. logarithmic true plastic strain plots of PD2-S fitted with various models, (b) Work hardening rate vs true plastic stress diagram..... 137

Figure 4.6: Linear fitting curves of the third stage in PD2-S using Kock, Mecking, (KM) based dislocation models. .... 140

Figure 5.1: (a) Calculated phase diagram of Fe-18Mn-XAl-1C-6Ni alloy system using Thermo-246 Calc (version 2022a) (The star mark indicates the homogenization temperature and oval mark indicates the annealing temperature), and (b) XRD pattern of the cast alloy. .... 143

Figure 5.2: Optical micrographs of steel of selected composition in (a) as-cast condition and (b) homogenized at 1200°C followed by hot rolling and water quenching (PD3). RD and TD indicate rolling and transverse directions, respectively. .... 145

Figure 5.3: Low-density steel after annealing of PD3 sample, at 930°C for 30 min followed by water quenching (PD3-A), (a) optical micrograph (b) SEM-secondary electron micrograph revealing different morphologies of B2 phase. The arrow indicates the respective precipitates..... 146

Figure 5.4: (a) X-ray diffraction patterns of PD3, PD3-A, and PD3-AB<sub>30</sub> samples..... 148

Figure 5.5: Phase maps (a, b, c), KAM maps (d, e, and f), and image quality maps with superimposed grain boundaries (g, h, i) for three samples: PD3, PD3-A, and PD3-AB<sub>30</sub>. The color indicators used are red for austenite and green for the B2 phase. Blue represents the strain-free region whereas green and red represent strained regions. .... 151

Figure 5.6: Misorientation angle vs. Number fraction chart of (a) PD3 (b) PD3-A and (c) PD3-AB<sub>30</sub> samples..... 156

Figure 5.7: (a) BF TEM micrograph of PD3-A showing austenite by a circle, (b) SAED pattern of austenite of encircled area in (a) along  $[022\bar{1}]$  zone axis, (c) BF TEM micrograph of PD3-A displaying B2 precipitates in austenite matrix, (d) SAED pattern of B2 platelet along  $[001]$  zone axis, (e) BF TEM micrograph of PD3-AB<sub>30</sub> revealing lamellar kappa carbide and ferrite at austenite grain boundaries. .... 157

Figure 5.8: (a) Engineering stress-strain diagram, (b) work hardening rate vs true plastic strain of PD3, PD3-A, and PD3-AB<sub>30</sub> samples..... 161

Figure 5.9: Experimental true stress- logarithmic plastic strain curves of (a) PD3 (b) PD3-A 435 and (c) PD3-AB<sub>30</sub> fitted with various flow equations ..... 163

Figure 5.10: SEM fractographs of the samples (a) PD3 (b) PD3-A and (c) PD3-AB<sub>30</sub> depicting cleavage facets and dimples. .... 164

Figure 5.11: Strengthening mechanisms responsible for strength contribution to yield strength.....	178
Figure 5.12: Experimental work hardening rate vs true stress in stage III and fitted curve as per KM model (Equation 5.13) for (a) PD3 and (b) PD3-A.....	181
Figure 5.13: Tensile properties of automotive steels (a) yield strength vs elongation and (b) tensile strength vs elongation. Corresponding properties of experimental steels are superimposed [6].....	183
Figure 6.1: (a) Optical micrograph, (c) secondary electron micrograph, and (e) magnified secondary electron micrograph of PD3-A sample depicting B2 platelets, globular B2 and banded B2 structures (as indicated by yellow arrows) in austenite matrix, (b) optical micrograph displaying deformed and fragmented B2 (d) secondary electron micrograph, and (f) magnified secondary electron micrograph of PD3-AE sample showing disintegrated, spheroidized B2 and B2 precipitate. ....	189
Figure 6.2: XRD patterns of PD3-A sample and PD3-AE samples conforming the presence of austenite and ordered B2 phases.....	192
Figure 6.3: Image quality map with superimposed grain boundaries of (a) B2 (c) austenite in PD3-A sample, partially recovered austenite is encircled by yellow line, (b) B2 (d) austenite in PD3-AE sample. ....	194
Figure 6.4: Number fraction vs misorientation angle of (a) B2 and (b) austenite in both PD3-A and PD3-AE samples. B2 is partly recovered, austenite is partially recrystallized. ....	196

Figure 6.5: Kernel average misorientation maps of austenite in (a) PD3-A with average KAM value of  $0.60^\circ$  and (b) PD3-AE sample with average KAM value of  $0.56^\circ$  suggesting the strain is reduced by electropulsing treatment..... 197

Figure 6.6: The orientation distribution function sections at  $\phi_2 = 0^\circ, 45^\circ, 65^\circ$  for B2 (a) PD3-A showing rotated cube texture components at positions of 1,2,3,4,5, and (b) PD3-AE. 199

Figure 6.7: Engineering stress-plastic strain curves of annealed (PD3-A) and electropulsed (PD3-AE) low-density steels and the tensile properties are shown in table in the inset. 201

Figure 6.8: SEM fractographs of (a) Annealed (PD3-A) sample showing cracks, dimples and facets (b) electropulsed sample (PD3-AE) displays cracks of finer size, dimples of larger size and higher area fraction with reduced amount of facets. ....202

Figure 6.9: Physical model of microstructures of (a) PD3-A, B2 bands(1, 2, 3, 8), globular B2 (4, 5, 10), B2 platelets (6, 7), recovery of austenite (9), different stages after electropulsing, PD3-AE, (b) dissolution of B2 (11-8I, 10 I), the disintegration of B2 spheroidization(10<sup>I</sup>) of B2, sublimation of austenite subboundary (9<sup>I</sup>), (c) spheroidization (1<sup>II</sup> -8<sup>II</sup>, 10<sup>II</sup>), nucleation of recrystallized austenite (9<sup>II</sup>), and (d) precipitation of B2 platelet (11), spheroidization of B2 (1<sup>III</sup> -8<sup>III</sup>, 10<sup>III</sup>) and growth of recrystallized austenite (9<sup>III</sup>). In Figure b-d, dotted boundaries are original boundaries and solid boundaries are boundaries after electropulsing.....215

Figure 6.10: Logarithmic true stress vs. logarithmic true plastic strain plots of PD3-A and PD3-AE samples (a) experimental, (b) &(c) experimental fitted with Hollomon, Ludwik, Ludwigson, Swift and Voce models and (d) work hardening rate vs true plastic strain diagrams for PD3-A and PD3-AE. Electropulsing reduces work hardening rate but increases ductility but decreases recovery. ....219

Figure 6.11: Linear fitting curves of (a) PD3-A and (b) PD3-AE samples using Kock, Mecking (KM) based dislocation models.....222

Figure 6.12: (a) Optical micrograph, (b) secondary electron micrograph of PD3-AB<sub>30</sub> sample depicting B2 platelets, globular B2 and banded B2 structures (as indicated by yellow arrows) in austenite matrix, (c) optical micrograph displaying deformed and fragmented B2 (d) secondary electron micrograph of PD3-AB<sub>30</sub>E sample showing disintegrated B2 and B2 precipitate.....224

Figure 6.13: XRD patterns of PD3-AB<sub>30</sub> sample and PD3-AB<sub>30</sub>E samples conforming the presence of austenite and ordered B2 phase, kappa carbide phases. ....227

Figure 6.14: TEM BF images of (a) PD3-AB<sub>30</sub> and (b) PD3-AB<sub>30</sub>E samples. ....229

Figure 6.15: Image quality map with superimposed grain boundaries of (a) B2 (c) austenite in PD3-AB<sub>30</sub> sample, (b) B2 (d) austenite in PD3-AB<sub>30</sub>E sample (the fraction of LAGB of misorientation angle <15° and HAGB of misorientation angle >15° are shown in inset).....231

Figure 6.16: Number fraction vs misorientation angle of (a) B2 and (b) austenite in both PD3-AB<sub>30</sub> and PD3-AB<sub>30</sub>E samples. B2 and austenite phases are partially recrystallized. ....233

Figure 6.17: Kernel average misorientation maps of B2 in (a) PD3-AB<sub>30</sub> with average KAM value of 0.65° and (b) PD3-AB<sub>30</sub>E sample with average KAM value of 0.62°, austenite in (c) PD3-AB<sub>30</sub> sample with average KAM value of 0.59° (d) in PD3-AB<sub>30</sub>E with average KAM value of 0.56° suggesting the strain is reduced by electropulsing treatment. ....234

Figure 6.18: Engineering stress-plastic strain curves of PD3-AB<sub>30</sub> and PD3-AB<sub>30</sub>E low-density steels. ....235

Figure 6.19: work hardening rate vs true plastic strain diagrams for PD3-AB<sub>30</sub> and PD3-AB<sub>30</sub>E.....238

Figure 6.20: Engineering stress-plastic strain curves of PD3-A, PD3-AE, PD3-AB<sub>30</sub> and PD3-AB<sub>30</sub>E low-density steels.....239

Figure 6.21: work hardening rate vs true plastic strain diagrams for PD3-A, PD3-AE, PD3-AB<sub>30</sub> and PD3-AB<sub>30</sub>E. ....241

## List of Abbreviations

UHSS	Ultra-high strength steels
AHSS	Advanced high strength steels
IF	Interstitial free steel
IF-HS	Interstitial free- high strength steel
Mild	Mild steel
BH	Bake hardenable steel
HSLA	High strength Low Alloy steel
DP	Dual phase steel
TRIP	Transformation Induced Plasticity Steel
CP	Complex phase steel
TWIP	Twinning Induced Plasticity steel
Med Mn	Medium manganese steel
MS	Martensitic steel
PHS	Press Hardened steel
QP	Quenched and Partitioned steel
RT	Room Temperature
mbar	milli bar
EDM	Electrical discharge machining
XRD	X-Ray Diffraction
SEM	Scanning Electron Microscope
FESEM	Field emission scanning electron microscope
EDS	Energy Dispersive Spectroscopy

EBSD	Electron Back Scattered Diffraction
TEM	Transmission Electron Microscope
MPa	Mega Pascal
GPa	Giga Pascal
Kg	Kilogram
Kgf	Kilogram force
kW	Kilo Watt
kHz	Kilo hertz
kN	Kilo newton
$\text{g/cm}^3$	Gram/ Cubic centimeter
$\text{J/mm}^3$	Joule / Cubic milli meter
$\text{mJ/m}^2$	milli joules / meter square
$\text{A/cm}^2$	Ampere / centimeter square
mm	millimeter
$\mu\text{S}$	micro seconds
$\mu\text{F}$	micro faraday
KV	Kilo volt
CRO	Cathode Ray Oscilloscope
EP	Electropulsing
P1	Fe-18Mn-6.5Al-0.75C
P2	Fe-18Mn-6.5Al-1.25C-2.5Ti
P3	Fe-18Mn-10Al-1C-6Ni
PD1	Fe-18Mn-6.2Al-0.75C (hot rolled)
PD1-S	Fe-18Mn-6.5Al-0.75C (solutionized)

PD1-SC	Fe-18Mn-6.5Al-0.75C (solutionized + cold rolled)
PD1-SCR	Fe-18Mn-6.5Al-0.75C(solutionized+CR+ annealed)
PD2-A	Fe-18Mn-6.5Al-1.15C-2.5Ti (solutionized)
PD3-A	Fe-18Mn-10Al-1C-6Ni (annealed)
PD3-AE	PD3-A + electro pulsed condition
PD3-AB <sub>30</sub>	Fe-Mn-Al-C-Ni (in aged condition)
PD3-AB <sub>30</sub> E	PD3-AB <sub>30</sub> + electro pulsed condition
ARCIS	Advanced Research Centre for Iron and Steel
YS	Yield strength
UTS	Ultimate tensile strength
PE	Plastic elongation
TE	Total elongation
PSE	Tensile toughness
LAGB	Low angle grain boundaries
HAGB	High angle grain boundaries
BCC	Body centered cubic
FCC	Face centered cubic
BCC_A2	Disordered ferrite
FCC_A1	Disordered austenite
BCC_B2	Ordered bcc
Fe <sub>3</sub> C	Cementite
SFE	Stacking fault energy
MBIP	Micro band induced plasticity
HEC	Hole expansion coefficient

BA	Bending angle
Ref	Reference
Y	Year
H	Homogenization
HR	Hot rolling
HF	Hot forging
CR	Cold rolling
An	Annealing
Sol	Solutionization
WQ	Water quenching
RPM	Revolutions per minute
CCPS	Capacitor charging power supply
mA	milli amperes
km	Kock, Mecking
$\theta_0$	Initial work hardening rate
$\frac{E}{\rho}$	specific stiffness
IQ map	Image quality map
KAM	Kernel average misorientation
ODF	Orientation distribution function
RW	Rotated W
RG	Rotated goss
VHN	Vickers hardness number
RD	Rolling direction

TD	Transverse direction
BF	Bright field
SAED	Selective area electron diffraction

## List of symbols

Fe	Iron
Mn	Manganese
Al	Aluminum
C	Carbon
Ni	Nickel
Cr	Chromium
Si	Silicon
Ti	Titanium
Nb	Niobium
Co	Cobalt
Mo	Molybdenum
Cu	Copper
V	Vanadium
B	Boron
NbC	Niobium carbide
TiC	Titanium carbide
SiC	silicon carbide
K	Kelvin
°C	Degree centigrade
B <sub>2</sub>	Ordered BCC precipitate
μm	Micro meter
κ	Kappa carbide

L	Liquid
$\gamma$	Austenite
$\alpha$	Ferrite
$\delta$	Ferrite at high temperatures
$\beta$	Beta manganese
$\kappa'$	Kappa carbide with in grains
$\kappa^*$	Kappa carbide at grain boundaries
$\gamma'$	Solute lean austenite phase
$\gamma''$	Solute rich austenite phase
W	Weight
$t_{hkl}$	Crystallite size
$e_{hkl}$	Micro strain
$\beta_L$	Lorentzian component of integral breadth
$\beta_G$	Gaussian component of integral breadth
$\lambda$	Wavelength
$\rho_{hkl}$	Dislocation density
b	Burgers vector
Å	Angstrom
E	Elastic modulus
G	Shear modulus
$\nu$	Poisson's ratio
$V_T$	Transverse velocity
$V_L$	Longitudinal velocity

$\rho$	Density
$\sigma$	True stress
K	Strength parameter
$\varepsilon$	True strain
n	Strain hardening exponent
$\sigma_s$	Saturation stress
$\sigma_i$	True plastic stress
$\sigma_P$	Peierls stress
$\sigma_D$	Dislocation strengthening
$\sigma_{SS}$	Solid solution strengthening
$\sigma_{GB}$	Grain boundary strengthening
$\tau_0$	Shear stress
M	Taylor factor
$K_B$	Grain boundary locking parameter
$a_0$	Lattice parameter
$\sigma_{Pr}$	Precipitation strengthening
D	Diameter of particle
$C_p$	Heat capacity
I	Current density
$(\Delta G_{Chem})$	Chemical free energy change
$\Delta G_{Inter}$	Interfacial free energy change